ELECTRONIC STRUCTURE OF ELEMENTAL BORON

A THESIS IN
Physics

Presented to the Faculty of the University
of Missouri-Kansas City in partial fulfillment of
the requirements for the degree

MASTER OF SCIENCE

by
Liaoyuan Wang

B.Sc., University of Science and Technology of China, 2001
M.Sc., University of Science and Technology of China, 2006

Kansas City, Missouri
2010

ELECTRONIC STRUCTURE OF ELEMENTAL BORON

Liaoyuan Wang, Candidate for the Master of Science Degree

University of Missouri – Kansas City, 2010

ABSTRACT

Boron has complex structures in its crystalline forms that lead to a variety of properties. The primary phases of elemental boron are α-B_{12}, t-B_{50}, γ-B_{28}, and β-B_{106} and are the focus of this thesis. As a preliminary step to elucidate the properties of these phases, *ab initio* calculations have been performed to obtain the electronic structure and optical properties of the system from a fundamental quantum mechanical point of view. Also calculated are the X-ray Absorption Near Edge Structure (XANES) spectra which can provide information about the relationship between atomic structure and electronic structure. The calculated XANES spectra of α-B_{12} agrees with experimental data in terms of peak position and peak height. Based on the success of the α-B_{12} calculation, XANES spectra of t-B_{50}, γ-B_{28}, and β-B_{106} are predicted. In addition, these XANES spectra are grouped according to the similar geometrical features that are present in their atomic structures and analyzed.

APPROVAL PAGE

The faculty listed below, appointed by the Dean of the College of Arts and Sciences have examined a thesis titled “Electronic Structure of Elemental Boron”, presented by Liaoyuan Wang, candidate for the Master of Science degree, and certify that in their opinion it is worthy of acceptance.

Supervisory Committee

Wai-Yim Ching, Ph.D., Committee Chair
Department of Physics

Michael Kruger, Ph.D.
Department of Physics

Anthony Caruso, Ph.D.
Department of Physics

Table of Contents

List of Illustrations

List of Tables

Table Page

ACKNOWLEDGEMENTS

I express my sincere gratitude and deep appreciation to my adviser, Professor Wai-Yim Ching. His patience, intelligence, and wisdom have been a guiding light during my research years at UMKC. Even more important was his encouragement and support in my professional and personal development. He helps me to overcome my faults in research and improve my research habits. Also, he provides me many chances to practice and encourages me to learn from failure. That he is serious and diligent in research inspires me to work hard.

A special thanks to Dr. Paul Rulis, from whom I got a lot of good advices and precious research experiences. I would like to thank Dr. Lizhi Ouyang who inspired me in many research topics and broaden my mind. I also appreciate my friends. You make my life easier and more joyful, and you accompany me through my hard times.

I appreciate my parents (Jinhua Wang & Guoxiang Wang) and my American parents (William Beard & Mary Beard). It is because of you that I can strive to reach a higher level and pursue my professional goals here. Thank you for accompanying me and helping me to go through my hard times. Your encouragement and help has inspire me to face all kinds of challenges and achieve the success in the past, present, and future.

I would also like to thank the other professors, staff members, and fellow students in the UMKC physics department for their help and friendship.

Financial support for my studies and research from the UMKC Department of Physics are gratefully acknowledged.

Dedicated to all those people who helped me.

CHAPTER 1

INTRODUCTION

1.1 Context

Boron-rich compounds attract the interest of many people due to their variety of features, such as high hardness, light weight, high neutron capture cross section and role in some superconducting materials. This has led to many applications or potential applications in a diverse range of areas such as armors, abrasives, nuclear applications, etc. [1-3]. A relatively unique feature of many boron-rich solids is a B_{12} unit in an icosahedral formation. Research shows that the hardness of boron-rich solids is related to this special structure [4]. Unfortunately, many of the outstanding properties of the various boron-rich compounds are still poorly understood because of the complex structures that can form. The limitations of current techniques increase the main difficulties for exploring the structures.

It is important to note that most phases of elemental boron and the boron-rich compounds have an icosahedral B_{12} unit as the fundamental building block [5-8]. Because elemental boron only has one type of element it is likely that this could reduce the complexity of researching it compared to studying the B-rich compounds. Although the structures of elemental boron are very complex, we choose to study elemental boron first before studying other boron-rich compounds for this reason.

1.2 Properties and Applications of Elemental Boron

Elemental boron has many unique combinations of properties. It tends to be hard but low density. The rhombohedral polymorph of boron is stronger than steel, harder than corundum, and lighter than aluminum. On the modified Mohr's scale, its hardness value is 11,

while diamond is 15 and boron nitride is 14 [9]. Hence, boron materials are often employed in heat-resistant alloys, as an abrasive in the process of cutting and polishing materials, etc. Recent research reveals that elemental boron exhibits superconductivity under high pressure[10-12]. From conventional theory, low-Z elements are beneficial for increasing the superconductivity transition temperature because of their high Debye temperatures; and of these materials, many require pressure to induce a superconducting state [10]. In addition, boron based solids are strong electron-phonon coupling systems and therefore potentially have high-T_c superconductivity [11]. Therefore, elemental boron has attracted great interest. In experiments, a particular allotrope of elemental boron, β-B_{106}, showed the onset of superconductivity at 160 GPa. The critical temperature of the transition increases from 6 K at 175 GPa to 11.2 K at 250 GPa.[10].

Elemental boron tends to be chemically inert and has a high-melting point. Another allotrope, α-B_{12}, is mechanically stable up to 1400°C, while β-Boron is thermodynamically stable up to 2450°C [13]. Isotopic boron is used in the protective coating of the walls of nuclear reactors and as control rods for neutron capture and shielding [9]. Due to this high heat resistance elemental boron is used in strong structural materials, abrasive tools, and as shielding for other materials under extreme conditions [3,14]. B-enhanced ceramics are used in nuclear reactors because they are effective neutron absorbers [3,15].The different allotropes of elemental boron can also be good semiconducting materials. β-boron inherently acts as a p-type semiconductor and can be made to be an n-type semiconductor by doping it with elements such as iron [9]. Their semiconducting properties facilitate their use as neutron detectors [16,17].

Filaments of boron, very thin threads or wires made by boron, have considerable tensile and flexural strength. Their response to stress tends to be entirely elastic, with no clearly discernible dislocation movements [9]. B and B-rich compounds also hold great promise for use in thermoelectric devices [18,19].

This list of outstanding and advantageous properties has led to the development of numerous practical applications, but many challenges remain. For example, current experimental techniques can not make pure elemental boron crystals to over 99.99% due to the existence of carbon, nitrogen, and oxygen due to variety of reasons, especially under high temperature and high pressure. As light elements, the energy onsets of X-ray Absorption Near Edge Structure (XANES) of boron, carbon, nitrogen and oxygen are very close while the current measurement techniques of X-ray absorption are unable to identify them well. Therefore, the experimental XANES spectra of boron measured include the spectra of defective elements, such as carbon, nitrogen, etc. These limitations in experiment increase the difficulties to explore the structures of elemental boron and boron-rich compounds.

1.3 The Role of Computational Physics

Computational physics is a bridge between experimental physics and theoretical physics that complements both. The goal of computational physics is to simulate real physical processes based on existing quantitative theories. This idea can be used to help conduct experiments, make predictions based on large-scale calculations, or even suggest new theories. The application of computational simulation helps us to understand observed phenomenon and properties[20,21].

1.4 Electronic Structure Methods

There exist many computational methods to calculate electronic structure. Examples include the tight binding method, nearly-free electron model, Hartree–Fock method, density functional theory (DFT), quantum Monte-Carlo methods, linear combination of atomic orbitals (LCAO) method, etc. [22]

Among these methods, DFT is one of the most popular and versatile available. Most results based on DFT agree with or are consistently related to many types of experimental data over a wide range of system sizes, types, and levels of complexity. This includes the band gap for insulators, magnetization, valence band optical properties, core level spectroscopy, cell geometry, internal parameters, etc. With this theory, the properties of a many-electron system can be determined by using a functional of the electron density to evaluate the exchange-correlation potential [23] which includes all terms except non-interaction kinetic energy and coulomb interactions. This part is the hardest one to determine and has to do some approximation.

1.5 Method of Calculation

The Orthogonalized Linear Combination of Atomic Orbitals (OLCAO) method, based on DFT in the local density approximation (LDA) has been applied to the calculation of the electronic structure and optical properties of many crystals with complex structures with large numbers of atoms [23-31]. In the OLCAO method, the crystal wave functions are expanded in terms of localized atomic orbitals which facilitates the interpretation of the calculated results [32,33]. All the atomic orbitals are expressed in terms of Gaussian-type orbitals (GTOs) while the potential function is expressed as a sum of atom-centered Gaussian functions. This

enables the rapid analytic evaluation of multi-center integrals [32,33]. In order to improve the efficiency and accuracy of calculation, the atomic orbital basis can be organized into three types, EB (extended basis), FB (full basis) and MB (minimal basis). Each basis set definition is typically used for different purposes. The MB consists of core orbitals and the occupied valence orbitals only [34]. The FB contains all core orbitals, all occupied valence shell orbitals, and one additional higher shell of orbitals. The EB extends the FB by adding one more higher shell of orbitals [34]. For example, the FB of boron includes 1s,2s,2p,3s,3p; the EB consists of 1s,2s,2p,3s,3p,4s,4p (here, 3d has not been included for its energy is much higher than 4s, 4p etc.); and the MB only includes 1s,2s,2p. For typical ground state calculations in OLCAO the orbitals of the core electrons are eliminated by the orthogonalization scheme to reduce the size of the secular equation. Core orbitals are usually identified as those that are lower than about -30 eV in energy because they do not play a large role in inter-atomic bonding. In boron, for example, the only core orbital is the 1s at -190eV.

The Vienna *ab initio* Simulation Package (VASP) is another DFT based computational package which performs *ab initio* calculations using pseudo-potentials and a plane wave basis set. It is very effective for force and total energy evaluation [25]. In this thesis, VASP is first employed to relax crystal structures to optimize the theoretical model to obtain the lowest total energy, then the electronic structure and XANES spectra of the elemental boron phase are calculated by using the super OLCAO method.

This thesis focuses on the electronic structure and X-ray Absorption Near Edge Structure (XANES) spectra of four allotropes of elemental boron, α-boron (B_{12}), γ-boron (B_{28}), t-boron (B_{50}) and β-boron (B_{106}). The atomic structure of each system (with the

exception of B_{106}) was obtained from published experimental data and then optimized by VASP. However, much higher purity (Slack[35] reported that the purity is up to 99.99%) crystal β-boron has not been obtained due to the limitations of preparing techniques[36]. Hence the structure of β-boron is still controversial. In addition, the partial occupation increases the difficulty of understanding the structure. Hence, the model of β-boron selected by this thesis is accepted without any relaxation. Later, the selection of the model of β-boron will be introduced. The electronic structure, bonding, and ELNES/XANES spectra for each system was then obtained from OLCAO. Compared to experimental XANES spectra of α-boron (B_{12}), the OLCAO method is proven to be credible. Based on this good agreement, we believe that the calculated results for γ-boron (B_{28}), t-boron (B_{50}) and β-boron (B_{106}) are good predictions. The comparison of the calculated results provides a good overview of elemental boron and it helps to lay a foundation of understanding for later study of related boron-rich compounds such as boron carbide, boron sub-oxide, boron nitride, etc.

CHAPTER 2

CRYSTAL STRUCTURES

Fig.1 is the phase diagram of elemental boron (Cited from Oganov's work) [37]. The phases of elemental boron are found over a wide range of temperatures and pressures and include α-phase, β-phase, γ-phase, t-phase and α-Ga type phase[37]. In this thesis, only first four phases will be discussed because they are available in experiment. The twelve boron atom icosahedral unit is a common feature of the four allotropes of elemental boron and most boron-rich compounds. Among these elemental boron, α-B_{12} and β-B_{106} have rhombohedral structures while t-B_{50} and γ-B_{28} have tetragonal structures.

2.1 Crystal Structure of α-B_{12}, t-B_{50}, and γ-B_{28}

α-B_{12}, which only includes one icosahedron in a primitive cell, has the simplest crystal structure of the elemental boron systems. It is helpful and useful to understand α-B_{12} before understanding the other allotropes of boron. Fig.2(a) shows the crystal structure of α-B_{12}. It is a rhombohedral primitive cell. A slightly distorted icosahedron is located at the corner of the rhombohedral unit cell [4,38]. α-B_{12} is characterized by two nonequivalent sites identified as polar (B_p) and equatorial (B_e) (see Fig.3). The B_p atoms form top and bottom triangular faces of an icosahedron [4] (Fig.3) and B_e atoms form a puckered hexagon in the plane perpendicular to the [111] axis [39]. B_p and B_e atoms are linked by two types of bonds, covalent bonds or three-center bonds (also named as three-center two-electron (3c-2e) bonds) in which three atoms are held together by two electrons [4,40]. Each B_p atom has six covalent bonds. Among them, five covalent bonds link to five nearest neighboring atoms in the icosahedron (intra-icosahedra) while the other links to a B_p atom of another icosahedron (inter-icosahedra). The

B_p forms relatively strong two-center two-electron (2c-2e) covalent bonds with the B_p of neighboring icosahedra; each B_e atom has five covalent bonds (see page 15 Table 1) which link in the boron atoms (B_p or B_e) in the icosahedra. There are two types of 3c-2e bonds discussed [4,38,41]. One type of 3c-2e exists in the intra-icosahedron [41], and the other exists among the inter-icosahedra [4,38]. Fujimori *et al* showed the existing 3c-2e bonds on the surface of icosahedron [42] . On the top and bottom, three B_p atoms form the 3c-2e bonds. He *et al* showed the B_e participate in planar 3c-2e bonds with the B_e of neighboring icosahedra. The 3c-2e bonds form equilateral triangles in the plane perpendicular to the [1 1 1] axis [38]. He *et al* reported that the distortion of B_{12} icosahedra results in the spatial asymmetry of the charge density on each boron-boron bond, and in the ionicity of B_{12} icosahedra [4].

Fig.2(b) is a view of tetragonal boron (t-B_{50}) along the c-axis [42]. It shows that there exist five types (labeled from B1 to B5) of atoms distributed to two kinds of units: icosahedral units and isolated boron atoms (labeled as B1). B2 atoms locate at the polar sites of icosahedra along $< 1\bar{1}1 >$. B1 located at the intersection of the $< 1\bar{1}1 >$ and the surface of the primitive cell. Each B1 (isolated boron) atom has two covalent bonds with two different B2 atoms. All atoms in icosahedron have six covalent bonds. Among these bonds, five covalent bonds link the nearest atoms in the icosahedra and the last one connects isolated boron or boron atom in the other different icosahedra. For example, five covalent bonds of B2 link to B3, B4, and B5 in the same icosahedron, and one covalent bond connects with isolated boron atom (labeled as B1).

γ-boron is one phase of elemental boron formed under high pressure. Fig.2(c) shows the crystal structure of γ-boron. It is also tetragonal and consists of two units: icosahedral units

(labeled from B2 to B5) and boron pair (labeled as B1). The arrangement of two units resembles a NaCl-type structure [37] if icosahedra and boron pair are treated like chloride ion and sodium ion respectively. Like t-B_{50}, all atoms of icosahedra have six bonds. Among them, five bonds link the nearest neighboring boron atoms in the icosahedra, and one connects with one atom outside icosahedra which could be one of boron pair or another boron atom in another icosahedron. Apparently, each atom of boron pair has two covalent bonds. One covalent bond links the pair of boron atoms, and the other one connects with the atom (labeled as B4) in an icosahedron.

2.2 Crystal Structures of β-Boron

The structure of β-boron is controversial [43], and a number of different models for it exist. The models are identified by the number of B atoms in a primitive cell with variations including B_{105} [7,9,43-45], B_{106} [15,44] , B_{315} [44]and B_{320} [35]. The source of the differences is the desire to use the language of crystallography to describe a complex system. The β-boron phase does not fall neatly into any common category because it contains B atoms in various interstitial sites and various intrinsic defects. These crystallographic problems are dealt with using the concept of partial occupation at certain crystal sites. Hoard's structure includes 16 types of crystal sites occupied by 105 boron atoms while Slack's structure includes 20 types occupied by 106 atoms. The types are labeled as B1, B2, B3, etc. There exist two different views about the gross structural units in these models. Callmer *et al* [9,45,46] observe that 105 B atoms can be considered as B_{84} + B_{10}-B-B_{10} in an intricate arrangement [9,47]. Jemmis *et. al* [9,15,47-49] instead view the system as a B_{57} (B_{28}-B-B_{28}) unit along the body diagonal with eight icosahedra located at the vertices of the rhombohedral cell, and twelve icosahedra located at the middle

of the edges of the cell [9,44]. Bonding considerations and electron counting indicate the condition of electronic deficiency for either β-B_{105} or β-B_{106}[15] and that the model should probably be constructed as B_{320}. However, Jemmis *et al* [9] have a different view. They state that the five-electron deficiency of an ideal β-boron unit cell which strictly falls in the space group $R\bar{3}m$ was the conclusion of band structure calculation. It can be understood by drawing parallels between boron-rich solids and polyhedral borane chemistry. This approach reveals that the polyhedral B_{57} unit has three electrons more than is needed for stability in its internal bonding network. Based on Jemmis's view, the partial occupancies of the icosahedral B_{12} framework atoms and the presence of interstitial atoms are necessary for the stabilization of the β-rhombohedral unit cell to satisfy the varying electronic bonding requirements[9]. Therefore, it is necessary to consider the effect of structural defects, such as vacancies and extra occupancies, in β-boron when the electronic structure is discussed. Setten *et al* [15] analyzed these structures by using density functional calculations in the generalized gradient approximation. After analyzing and comparing Hoard's and Slack's structures, they claim that the most stable structure based on thermodynamic grounds is a 106 atom structure with one B13 crystal site vacant and two B atoms added at specific B16 crystal sites .Therefore, this thesis selected Setten's model as the representative of β-boron based on Jimmis's work and Setten's works.

Fig.4 is the crystal structure of β-B_{106} [50] . Fig.4(a) shows the primitive cell. Some specific sites, B1(green), B2(green), and B8(red), will be discussed in relation to the electronic structure and XANES spectra later. In this figure, different colors represent different groups. Orange represents corner icosahedra. Light green is for an interstitial boron.

Red is for the single boron between two clusters. Blue, dark green, and plum colors represent icosahedra located at edges A, B, and C respectively. Pink atoms represent complex clusters T1 (upper (28 atoms)) and T2 (lower (27 atoms)). Here, T2 is an open cluster due to one atom missing. This configuration disagrees with the ideal B_{28}-B-B_{28} model mentioned early because Setten's model is distorted thermodynamically to obtain the lowest total energy. In Fig.4 (a) only the atoms in the primitive cell are shown, and the icosahedra cannot be seen clearly. Fig.4 (b) instead includes atoms from the neighboring cell and clearly shows that there are single icosahedral units located at the corners and edges of the rhombohedral unit cell. Further, two complex clusters that are formed by three face-contacted icosahedra and two interstitial boron atoms (green; labeled as B1 and B2) can be seen connected to a single boron atom (red; labeled as B8) at the cell center. Fig.4 shows the local nearest neighbors of B1(or B2) and B8 are very different. These features could be observed later in PDOS and XANES spectra. The structure has been relaxed fully using VASP and does not have any symmetry. Therefore, the space group is P1. The number of the nearest neighbor atoms for each boron in β-B_{106} ranges from 4 to 8, which is very different compared to the first three phases, α-B_{12}, t-B_{50} and γ-B_{28}.

β-B_{106} in this thesis has 106 types of boron sites due to the distorted structure. The complicated structure increases the difficulty to understand it. Each boron atom in a given icosahedron covalently bonds with another boron atom in a different icosahedra or cluster.

Table 2 shows the lattice constants of the four phases of elemental B we studied. These structural data determine their electronic structure. Later, band structure, partial density of state, and XANES spectra based on these information will be discussed. Table 3 shows

structural features in four boron crystals. There are respectively 2, 5, 5, and 106 types of nonequivalent sites in α-B_{12}, t-B_{50}, γ-B_{28}, and β-B_{106}. The bond numbers of each phase are also listed in Table 3.

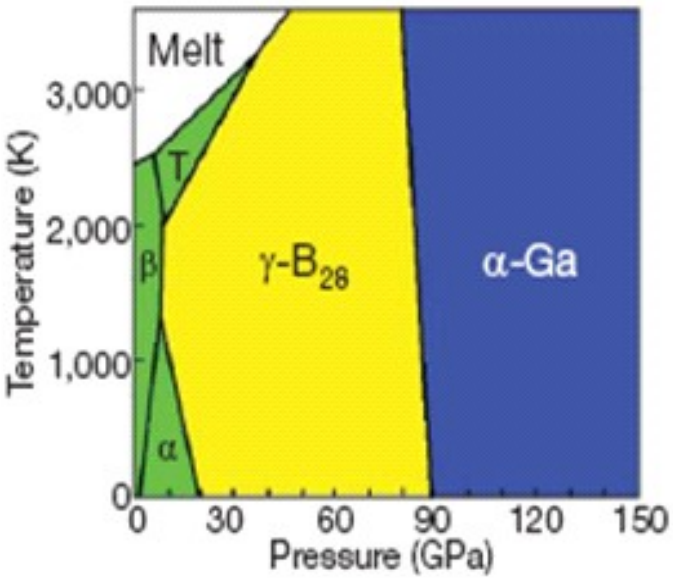

Fig.1 Phase Diagram of Boron [38]

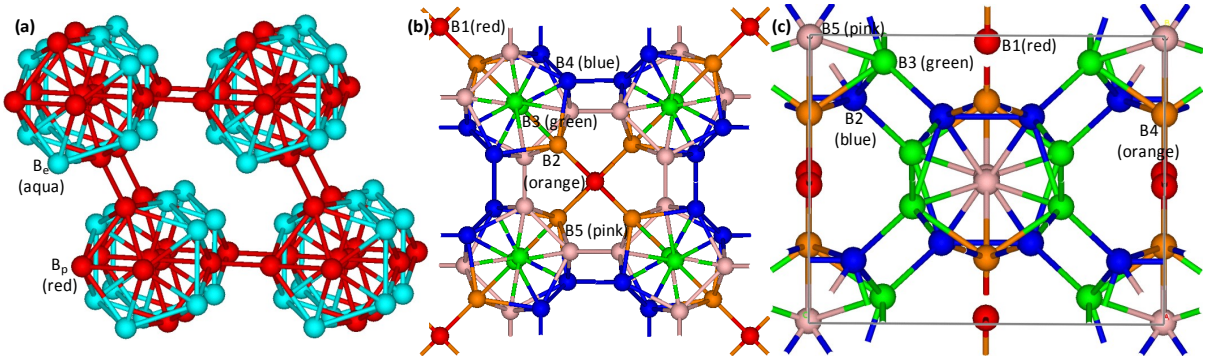

Fig.2 Crystal Structure of (a) α-B_{12}, (b) t-B_{50}, and (c) γ-B_{28}

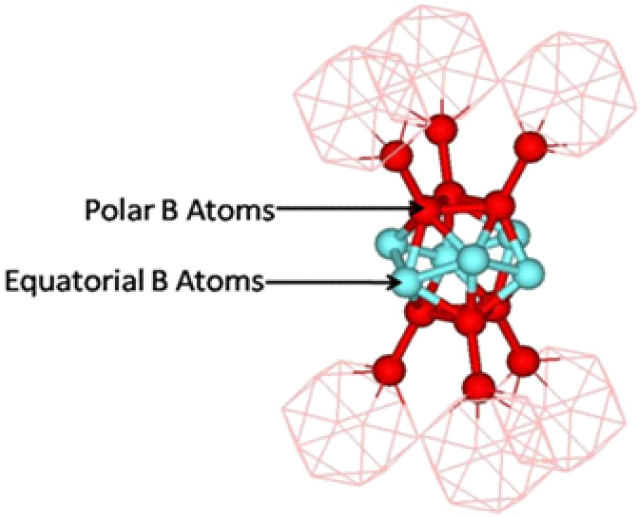

Fig.3 Polar and Equatorial Boron in α-B_{12}

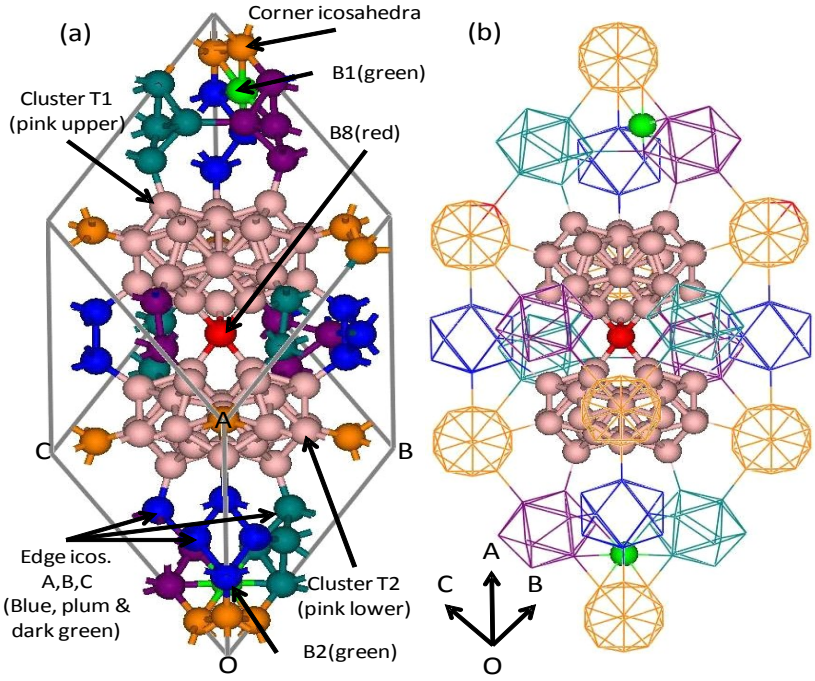

Fig.4 Crystal Structure of β- B_{106} (a) Primitive Cell, (b) Primitive Cell with Atoms from Neighboring Icosahedra

Table 1 Bond Length of α-B_{12}

	B_p (Å)	B_e(Å)
B_p	1.6562; 1.7247(2)*	1.7701; 1.7781(2)
B_e	1.7701; 1.7781(2)	1.7599(2)

* The number in bracket is the amount of bonds with same bond length.

Table 2 Lattice Constants in Four Boron Crystals

Name	a（Å）	b（Å）	c（Å）	α	β	γ	Space group number
α-B_{12} [51]	4.93	4.93	12.56	90°	90°	120°	166
t-B_{50} [42,51]	8.74	8.74	5.03	90°	90°	90°	134
γ-B_{28} [37]	5.04	5.61	6.92	90°	90°	90°	58
*β-B_{106} [15]	10.1	10.15	10.14	65.03°	65.07°	65.19°	1

(* This structure was relaxed by VASP, therefore the space group in the thesis is 1.)

Table 3 Structural Features in Four Boron Crystals

	Numbers of nonequivalent B sites	Number of Nearest Neighbor Bonds
α-B_{12}[51]	2	5,6
T-B_{50}[42,51]	5	2,5,6
γ-B_{28}[37]	5	2,5,6
β-B_{106}[15]	106*	4,5,6,7,8

*Due to the disorder structure, all atoms in β-B_{106} are nonequivalent.

CHAPTER 3

RESULTS AND ANALYSIS

3.1 Band Structure and Density of States (DOS)

Fig.5 shows the calculated electronic band structure of α-B_{12}, t-B_{50}, γ-B_{28}, and β-B_{106}. The red line represents Fermi Level. Based on the calculation of band structure, α-B_{12}, γ-B_{28}, and β-B_{106} and they are considered as semiconductors, while t-B_{50} is a metal. The direct band gaps at Γ for α-B_{12}, γ-B_{28}, and β-B_{106} are 3.3 eV, 3.2 eV, and 1.83 eV respectively, while the indirect gaps are 2.61 eV, 2.10 eV, and 1.75 eV respectively. Previous calculations on α-B_{12} produced indirect band gaps of 1.4-2.0 eV, and direct gaps from 1.8 to 2.6 eV [15,29,52,53]. On the basis of optical experiments, Horn [15] suggested a (direct) gap of approximately 2.0 eV. Ternauchi [54] *et al*. derived a (direct) optical gap of 2.4 eV based on electron energy loss experiments. Our calculated results agree with the experimental data reasonably well. For α-B_{12}. the top of the valence band is located at A point while the bottom of the conduction band is at the M point. Fig.5(b) shows that the top of the valence band of γ-B_{28} is located at the Γ point and the bottom of the conduction band is at the Z point. The top of the valence band in β-B_{106} is located at the Γ point while the bottom of the conduction band is at the Z point (Fig.5(d)). Fig.5 shows that the top of the valence band states of γ-B_{28} and β-B_{106} are flatter than those of α-B_{12}. It means that the effective mass of the charge carrier is smaller in α-B_{12} than in γ-B_{28} and β-B_{106}. The widths of valence band are 9.72 eV, 11.68 eV, 13.07 eV, and 9.7 eV for α-B_{12}, t-B_{50}, γ-B_{28}, and β-B_{106} respectively (refer to page 25 Table 4).

Fig.6 (a) compares the total density of states of α-B_{12}, t-B_{50}, γ-B_{28}, and β-B_{106}. Total DOS (TDOS) of t-B_{50} shows it to be metallic and the upper valence bands are unoccupied (the

vertical line at zero energy is the Fermi Level). For α-B_{12}, t-B_{50}, and γ-B_{28}, the lowest peak at -16 eV comes predominantly from boron 2s with some mixing from p orbitals based on our orbital resolved density of states which have not been shown here. However, in the case of β-B_{106}, there are multiple peaks in the range, reflectting the complexity of local atomic arrangements. TDOS of β-B_{106} shows there is a defective state in the band gap which will be discussed later. Fig.6(b) is the DOS of α-B_{12}. It shows that at the top of the valence band, the polar sites primarily contribute much more than the equatorial sites, and at the bottom of the conduction band, the equatorial sites contribute more. The DOS of t-B_{50} (Fig.6(c)) shows that each site contributes to the top of the unoccupied valence band. This feature affects the XANES spectra of t-B_{50} to be discussed later. The unoccupied valence states are primarily contributed to by B1 (isolated boron), B2, B3, and B4. The positions of the valence band unoccupied states of B1 and B2 are very close, while the rest of them are much closer to Fermi level. At the deep energy level (around -16 eV), the density of states of B1 has little contribution, while the contribution from B2 to B5 is very high. Fig.6(d) is the DOS of γ-B_{28}. Similarly, atoms labeled B1 are boron pairs. At the deep energy level (around -17 eV), the density of states of B2 and B3 is much stronger than the others. Particularly, the density of states of B1 is zero.

As for β-B_{106}, due to too many types of atoms in the primitive cell, the PDOS of some special sites of β-B_{106} are selectively shown in Fig. 7, Fig.8, and Fig.9. Here, by resolving into partial density of states (PDOS), the distribution of states could be identified well. From the total density of states of β-B_{106}, there is a defective state in the gap. Analysis of the PDOS shows that the defective state is contributed to by 23 atoms. The decomposed partial density

of states shows that the state comes primarily from atoms labeled as B85, B92, B97, B104, etc. Fig. 7(a) shows the location of these atoms responsible for the defective state in the band gap. Based on the contribution from high to low, these atoms are marked different colors: green, blue, red and orange. Apparently, these atoms belong to the complex cluster T2. Fig. 7(b) and Fig. 7(c) shows that these atoms do not contribute much to the bottom of the conduction band. Fig.8 shows the PDOS of isolated boron atoms in the primitive cell. Both atoms, B1 and B2, have similar local environments. There are many common features in their PDOS, while the PDOS of B8 which is positioned between cluster T1 and T2 is very different from B1 or B2. B8 contributes very little to the top of the valence band and the bottom of the conduction band. At the deep energy level, B8 contributes to the peak labeled "a", while B1 and B2 contribute to the peak labeled "c". Fig.9 is the grouped PDOS of β-B_{106}. The primitive cell of β-B_{106} can be seen to have different compositional units, the PDOS of each distinct unit is shown in Fig.9. The label "corner" refers to the PDOS of all atoms of all the icosahedra at the corners; "Total Edge" is the sum of the PDOS of all edge icosahedra; "Edge A", "Edge B" and "Edge C" are PDOS of icosahedra located at the OA, OB, and OC axis, respectively. "T1" and "T2" are PDOS of cluster T1 and T2. It clearly shows that the defective state mainly comes from the cluster T2. At the deep energy level, peak a is from cluster T1, peak b is from cluster T2, and the peak c is from the corner icosahedra.

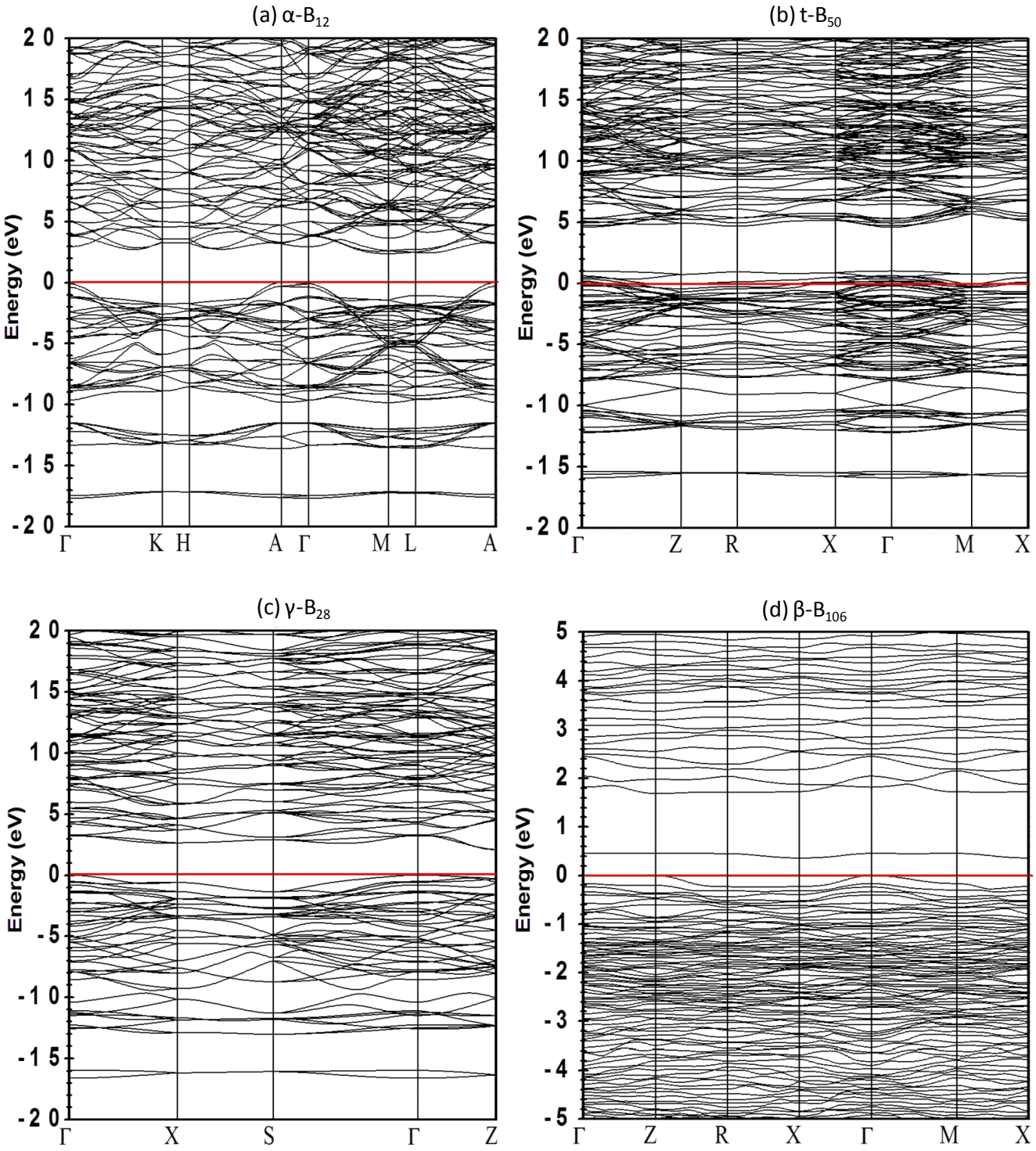

Fig.5 Electronic Band Structure of (a) α-B_{12}, (b) t-B_{50}, (c) γ-B_{28} and (d) β-B_{106}

(Red line represents Fermi Level)

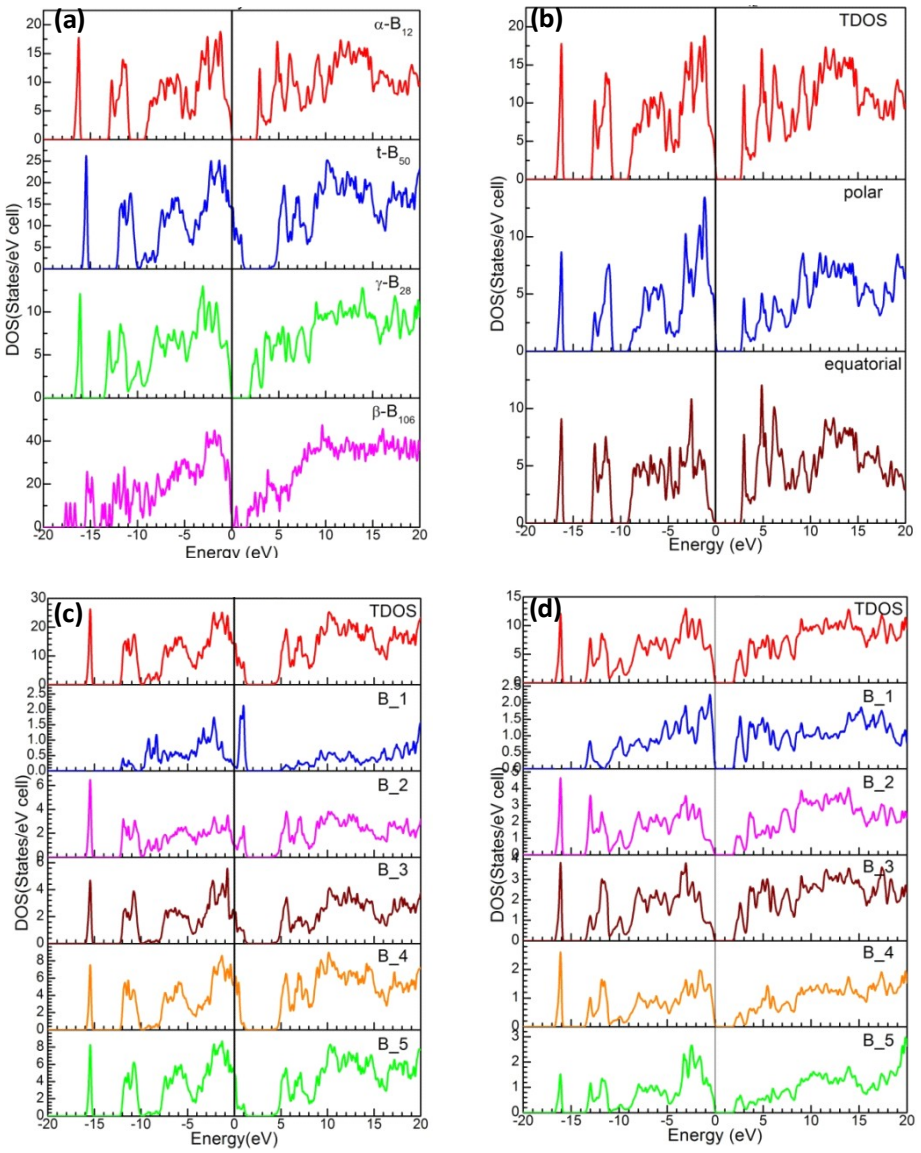

Fig.6 (a)TDOS of α-B_{12}, t-B_{50}, γ-B_{28} and β-B_{106}; Site-decomposed PDOS of (b) α-B_{12}, (c) t-B_{50}, (d) γ-B_{28}

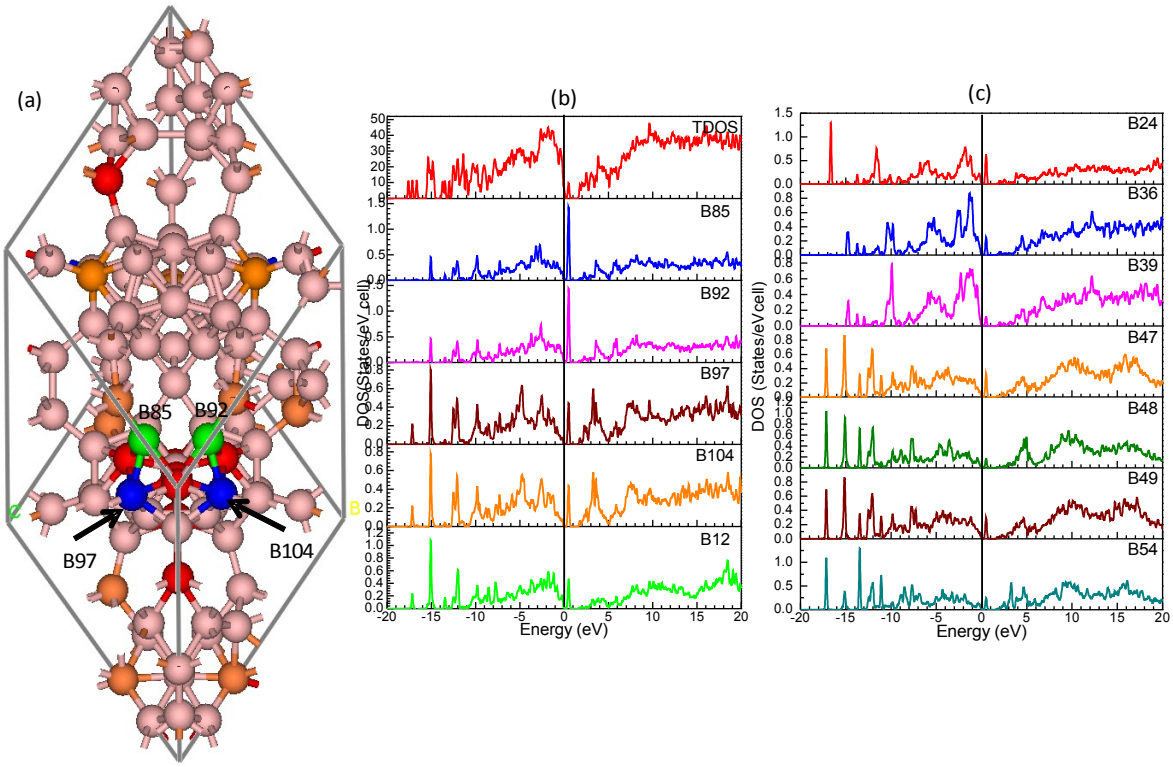

Fig. 7 PDOS of β-B_{106} (a) Location of Atoms Contributed to Defective State are Mark Green, Blue, Red, and Orange Color. Green: B85, B97; Blue: B97, B104; Red: B12, B24, B36,B39, B47, B48, B49,B54; Orange: B14, B15, B16, B28, B32, B33, B35, B74, B75, B76, B77; (b) (c) PDOS of Defective-State-Contribution Atoms of β-B_{106}

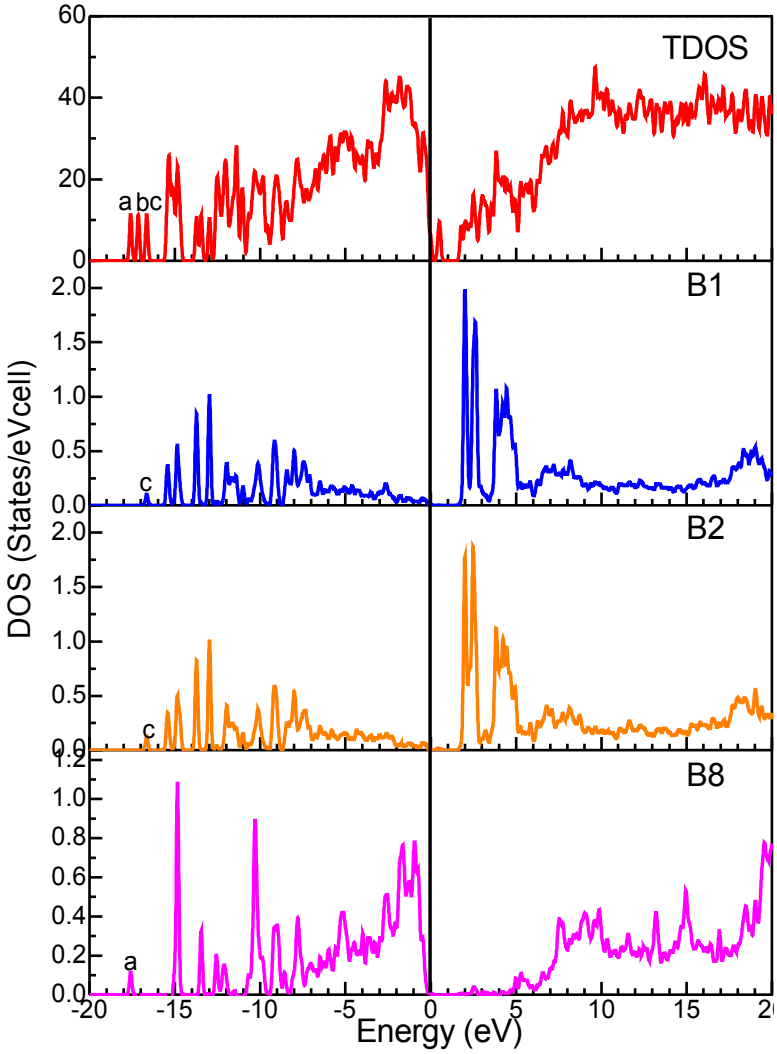

Fig.8 PDOS of Specific Sites (Single Boron) in β-B_{106}

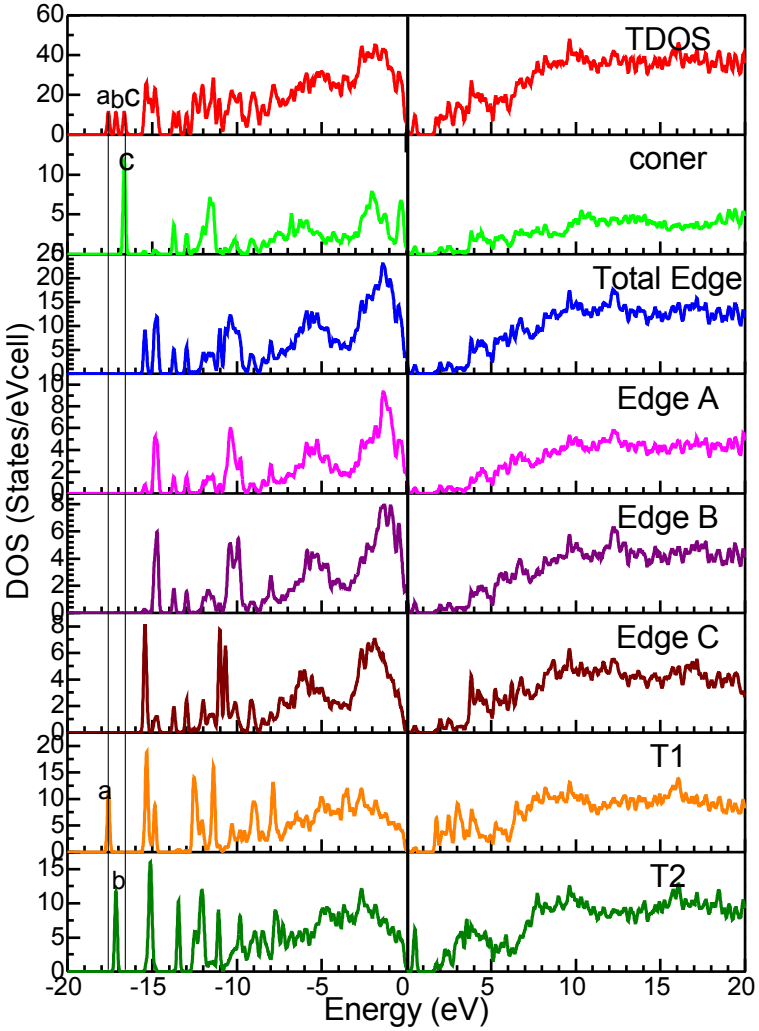

Fig.9 Grouped PDOS of β-B_{106}

Table 4 Calculated Band Gaps in Four Boron Crystals

	α-B_{12}	t-B_{50}	γ-B_{28}	β-B_{106}
Direct Band Gap at Γ (eV)	3.3	-	3.2	1.83
Indirect Band Gap (eV)	2.6	-	2.1	1.75
Super-cell used(No. of atoms/super-cell)	2X2X 2(96)	1X1X2 (100)	2X2X 2(244)	1X1X 1(106)
Upper valence band width(eV)	9.72	11.68	13.07	9.7

3.2 X-ray Absorption Near Edge Structure (XANES) Spectra

3.2.1 Introduction

X-ray Absorption Near Edge Structure (XANES) spectra, also Near Edge X-Ray Absorption Fine Structure (NEXAFS), was developed in the 1980s with the goal of elucidating the structure of molecules bonded to a surface, especially low-Z elements, such as carbon, nitrogen, oxygen, etc. XANES is sensitive to the local environment which is actually determined by the crystal structure. Therefore, it is natural to consider the correlation between XANES and crystal structure. Generally, the crystal structure can be quantitatively identified by the bond length, bond angle, the amount of bonds, the nearest neighboring atoms (may be different elements) symmetry, geometric group (for elemental boron, it is icosahedra), and so on. In this thesis, the correlation between XANES and the amount of bonds will be discussed.

The super-cell OLCAO method is employed to calculate XANES spectra [34] due to its good efficiency and acceptable accuracy. Following steps are performed to calculate XANES spectra. First, a super-cell is crated based on the size of the primitive cell. If the size of a primitive cell or super-cell selected is too small, the interaction of core-hole in each primitive cell or super-cell will distort the spectra. Hence, a super-cell should be used to eliminate this interaction. For example, the primitive cell of β-B_{106} is sufficiently large itself and can serve as a super-cell. While the primitive cell of α-B_{12} is not large enough so that the super-cell is introduced in the calculation. The super-cell sizes for α-B_{12}, t-B_{50}, and γ-B_{28} are 2x2x2, 1x1x2, and 2x2x2 respectively. Exact values are listed in Table 4.

Second, one target atom is identified and its neighbor atoms are labeled by different types of sites based on a selected sphere centered on the target atom. As well known, for prefect crystal structures with symmetry, there exist those sites named crystallographic sites which are equivalent in a same crystal structure. However, when XANES are performed by the super-cell OLCAO method, a sphere centered on the target atom is selected. Within the sphere, atoms are treated as different sites no matter whether they are crystallographically equivalent or not. Outside the sphere, atoms are treated as regular crystallographic sites. This greatly reduce the calculation scale, also, the local information will not be omitted.

Third, the calculation of the initial state (also called as ground state: GS) of the targeted atom will contain its core states. The final state (also called as excited state:ES) is obtained by removing one electron from the core state of the target atom and placing it in the lowest unoccupied state and solving the resulting Kohn-Sham equation self consistently. In this way, the core-hole effect is accounted for. Then the transition probabilities from the core level ground state to the unoccupied excited states are calculated, and the energy onset is shifted by using the equation TE_{GS}-TE_{ES} (TE: total energy). Finally, the calculated XANES spectra is normalized to unit area. The total XANES spectrum is the weighted sum of individual spectra for all nonequivalent sites. Later, an example based on the α-B_{12} will be briefly shown.

Obviously, above process of XANES calculation shows XANES spectra will be affected by the local structures which primarily comes from the atoms in the sphere.

3.3.2 XANES Calculation of α-B_{12}

Fig.10 is the XANES spectra of α-B_{12} calculated by using the OLCAO method. It is well

known that α-B_{12}, includes two types of sites, polar and equatorial sites (crystallographic sites). Both of them have 6 atoms in the crystal. First, polar site is selected as target atom and a sphere with 3 Å radius is selected. Within the sphere, the boron atoms including polar and equatorial are treated as different sites; outside it, those boron atoms are considered as their original crystallographic sites (polar or equatorial sites). After exerting two step calculations above mentioned, the XANES spectra of polar site then so does the equatorial sites. XANES spectra of them are shown in the second and the third panel of Fig.10. Due to the same atomic amount, the weight factor of polar and equatorial sites is both 0.5. Each spectroscopy is added with the weight factor to get the total XANES spectra of α-B_{12} shown in the first panel of Fig.10.

There is a pre-edge peak at 193 eV. The B-K edge of the polar site and equatorial sites have similar peaks and inter-peak energy separations. However, when combined, the different relative peak heights and energy on-sets lead to a total B-K edge that is substantially different from either the individual polar or equatorial K-edges. The pre-edge comes from the polar B sites. Both sites contribute to peak A'. However, only equatorial sites contribute to peak A" of the total B-K edge and the polar sites contribute to peak A"' of the total B-K edge. Peak B of the total B-K edge is from both equatorial sites and polar sites.

Fig.11 is the comparison of experimental [54] and computational XANES spectra of α-B_{12}. The calculated result was shifted to a lower energy by 4.09 eV to match the calculated main peak with the main peak from the experimental data. Terauchi *et* show that the onset of α-B_{12} is at 188.6 eV while that of the calculated result is at 188.9 eV. The experimental structure,

reported by Terauchi *et*, has seven prominent peaks. Although the calculated one has more peaks, the location of peaks agree with the experimental data. The outline of the calculated data agrees with that of the experimental data in the range of 185-230 eV. They both have a clear pre-edge and almost the same configuration of peak positions and intensities. The success of this calculation encourages us to used computed XANES spectra of t-B_{50}, γ-B_{28}, and β-B_{106} as predictions.

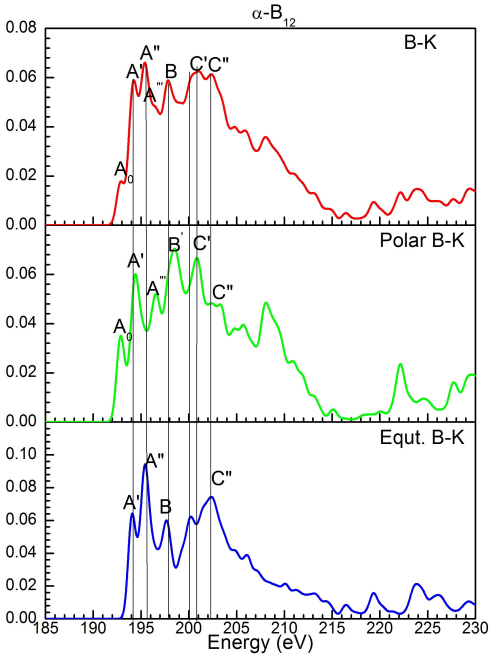

Fig.10 Decomposed XANES Spectra of α-B_{12}

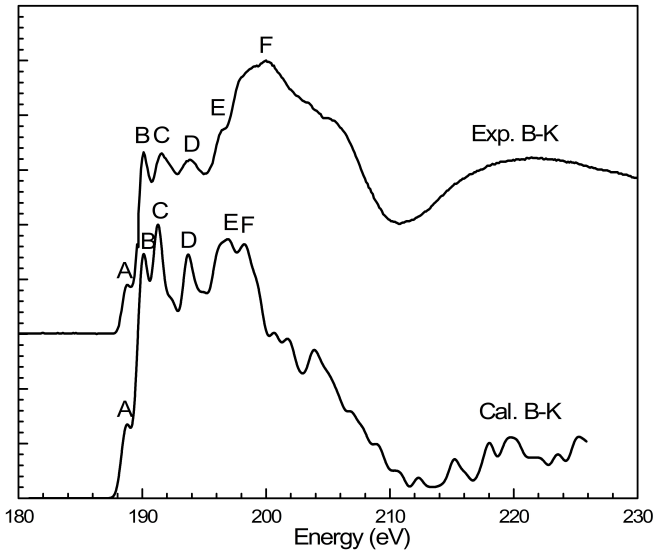

Fig.11 Comparison of Experimental and Calculated XANES Spectra of α-B_{12} [54]

3.2.3 XANES spectra of t-B_{50}, γ-B_{28}, and β-B_{106}

Next, we use the super-cell OLCAO method to calculate and predict the XANES spectra of t-B_{50}, γ-B_{28}, and β-B_{106}.

The XANES spectra of t-B_{50} (Fig.12) shows that there are small peaks before the main rising edge. They are contributed to by each nonequivalent site. The "bump" peaks exist due to the unoccupied states at the top of the valence band. The PDOS of t-B_{50} (page 21 Fig.6(c)) shows that each site contributes to the unoccupied top of the valence band. In Fig.12, the XANES spectra of the isolated boron (B1) is substantially different from the other sites. The XANES spectra of each site in the icosahedra has similar features although the locations of the primary peaks are different. .

Fig.13 shows the XANES spectra of γ-B_{28}. Obviously, the B-K edge of the boron pair (labeled as B1) is very different from the other B-K edges. The pre-edge comes from B4 and B5. Similarly to t-B_{50}, the general structures of B2–B5 are somewhat similar. However, the relative peak heights are all very different. Beyond the general spectra, the specific peaks and valleys in the spectra are almost impossible to explain in a simple way because of the difficulties of finger printing when the system of interest is complex [27]. Qualitatively though, some comparison between α-B_{12} and γ-B_{28} spectra can be made because the two systems retain substantial similarities. Structurally, B_p is more similar to B4 and B5, and this bears out in the comparison of their spectra [27]. B4 and B5 have the same distinct small first peak and lower energy on-set [27]. This also holds true for a comparison of B_e and B2, B3. These spectra have a more intense initial 3-4 eV and a higher energy on-set.

β-B_{106} model has 106 nonequivalent sites. All 106 spectra were calculated but the

decomposed XANES spectra cannot be fully shown. Considering that XANES is sensitive to the local environment, the grouped decomposed XANES spectra based on the nearest neighbor bond-number and geometrical structures are shown in Fig.14 and Fig.15. In the figure, "icos. at corner" refers to the icosahedra at the corner of the rhombohedral structure. "Edge tot." refers to the icosahedra located at the middle of the edge. "T1" is a cluster which includes 28 atoms in the rhombohedral structure, and "T2" is another cluster which includes 27 atoms. The nearest neighbors are determined based on the bond length. Here, we select the scale between 1.5 Å and 1.9 Å. In the β-B_{106} primitive cell 5 atoms have 4 nearest neighbors (NN); 15 atoms have 5 NN; 65 atoms have 6 NN; 13 atoms have 7 NN and 9 atoms have 8 NN. Fig.14 shows the total B-K edge and the bond-number grouped B-K edge. The total spectra shows an unclear pre-edge. The decomposed spectra shows that it is mainly from those atoms with 6 bonds. Fig.14 also shows that the B-K edge of sites with 4, 5, or 6 nearest neighbors have similar spectra, however those sites with 7 and 8 bonds have rather different features. Fig.15 shows the grouped XANES spectra based on the geometrical structures. It shows XANES spectra of icosahedra at the corner and the edge, although they have the same number of atoms and similar geometrical structure, they are apparently different. Due to the difference of atomic amount of icosahedra at corners and edges, the spectra are very different. Intensity of spectra of the edge icosahedra is much larger than that of the corner icosahedra. T1 and T2 have similar structures and absorption intensity. However, T1 has one more atom than T2. The XANES spectra are apparently different. The XANES comparison of single icosahedron at different location (see Fig.16) shows the substantial difference of XANES spectra. These single icosahedra all have the same amount

of boron atoms and similar geometrical structures, however, the apparent difference shows the effect of local environment. The analysis of bond length and bond angle shows that each icosahedron at different locations is distorted. And they have different neighboring circumstance. Hence, this difference could be understood.

In the band structure section (page 17 section 3.1), the decomposed PDOS showed the contribution of some special sites. Fig.17 shows the XANES spectra of these sites. The top panel is the total XANES spectra of β-B_{106}, the second panel shows the XANES spectra of the sites contributing to the defective states, and the bottom panel shows the XANES spectra of the primary sites which contribute the most to the density of states of the defective state in band gap. The pre-edge shows that it is in terms of the unoccupied defective state.

The elemental boron system we considered only includes one kind of element, boron, and similar geometrical units, icosahedra. In all phases, most boron atoms are in icosahedra, and a few atoms fill in the space between icosahedra like interstitial atoms. It is very reasonable to compare these groups of spectra together to find any interesting relationships. Fig.18 shows the different XANES spectra of different single boron atoms or boron atom pairs. Metallic B_{50} has unoccupied valence band states and the single boron in the B_{50} primitive cell also has unoccupied states at the top of the valence band. Therefore, its XANES spectra is apparently different from the others. B1 and B2 of β-B_{106} have very similar local environments (refer to page 14 Fig.4). B8 bonds with the cluster T1 and T2. Its local environment is very different from B1 and B2. Their XANES spectra are remarkably different from each other.

Fig.19 shows XANES spectra of all icosahedra in different phases. If α-B_{12} is selected

as a reference sample because it only has one icosahedral structure, the XANES spectra of γ-B_{28} can be seen to be similar to it. This means that the effect of the boron pair to the icosahedra is small. Similarly, the corner icosahedra of β-B_{106} has a similar spectra to that of α-B_{12}, whereas XANES spectra of edge icosahedra are rather different due to the variation in local environment, the distortion of icosahedra, and other unknown reasons. Comparing XANES spectra of t-B_{50} and γ-B_{28}, both have tetragonal structures, their XANES spectra are very different due to some unknown reasons.

Fig.20 shows the total B-K edge of the four phases to get an overview. If α-B_{12} is selected as reference sample, the rest of spectra could be compared to it. These total spectra looks very different. Based on the calculation (without shift), the onsets of α-B_{12}, t-B_{50}, γ-B_{28}, β-B_{106} are 191.8 eV, 193.8 eV, 193.2 eV, 191.3 eV respectively. Before the pre-edge, t-B_{50} exhibits different structure for it is metallic (refer to the band structure section). Except for t-B_{50}, the other phases show the pre-edge existing. The difference is related to the structure apparently due to the unique element. Also, the local structure affect the total spectra based above analysis.

.

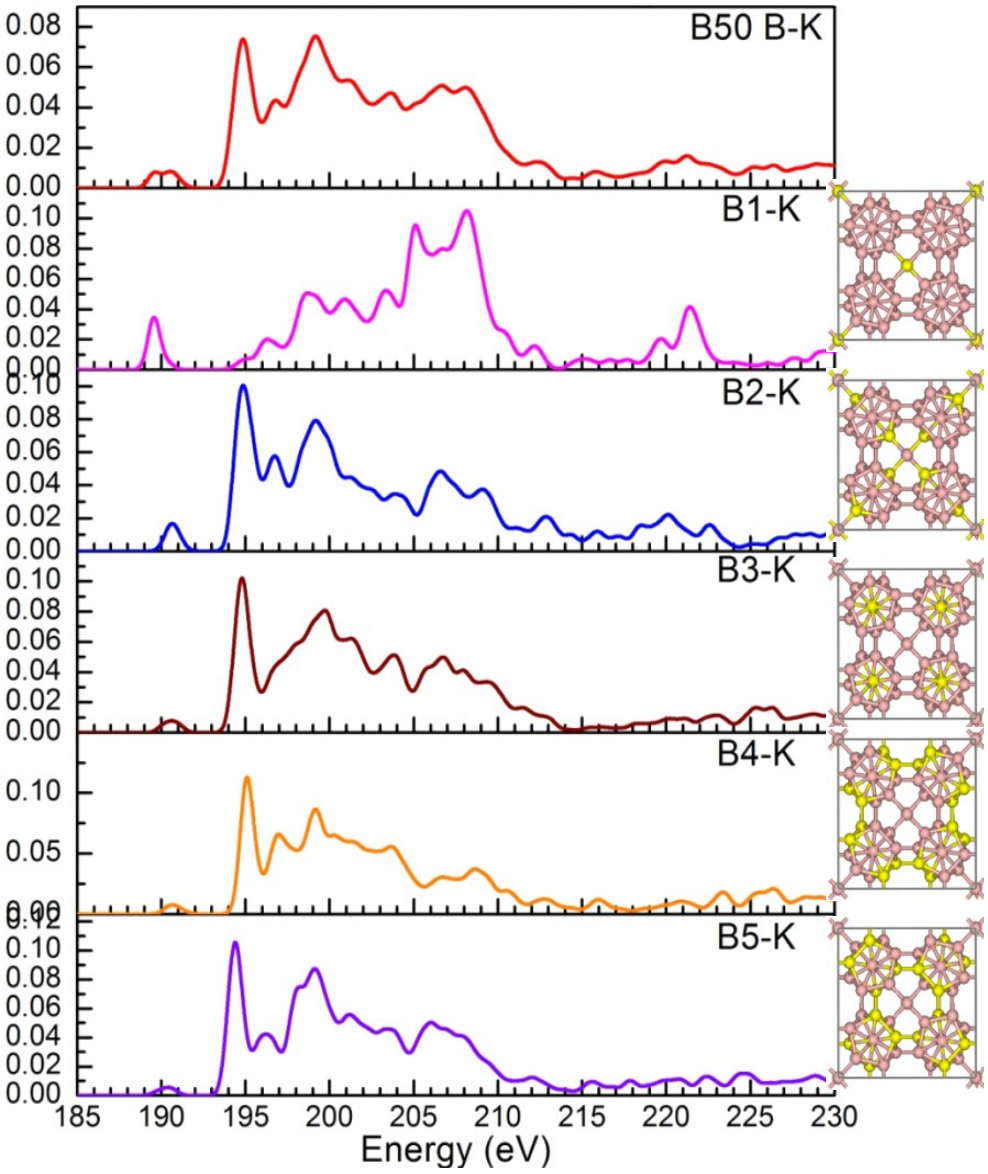

Fig.12 Decomposed XANES Spectra of t-B_{50}

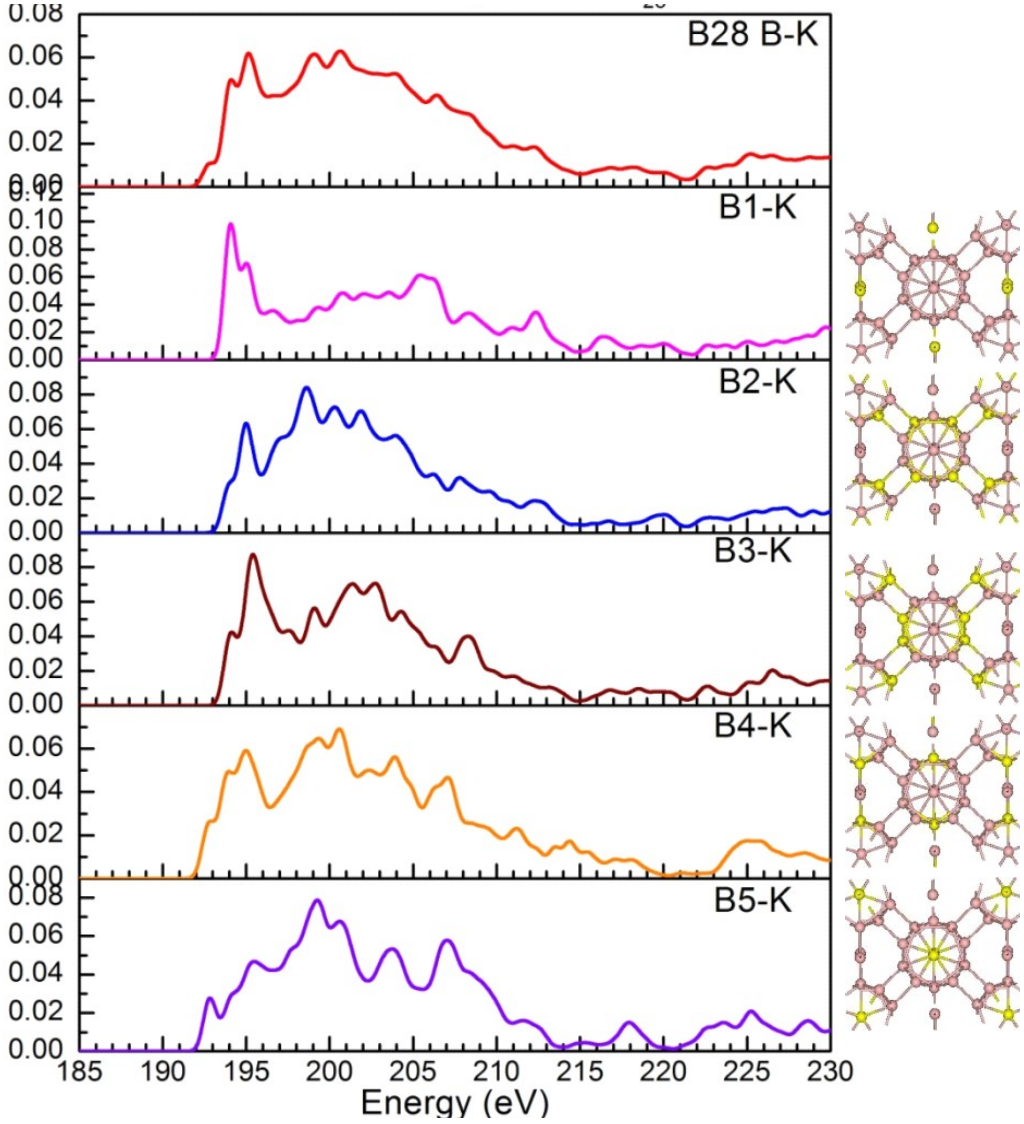

Fig.13 Decomposed XANES Spectra of γ-B_{28}

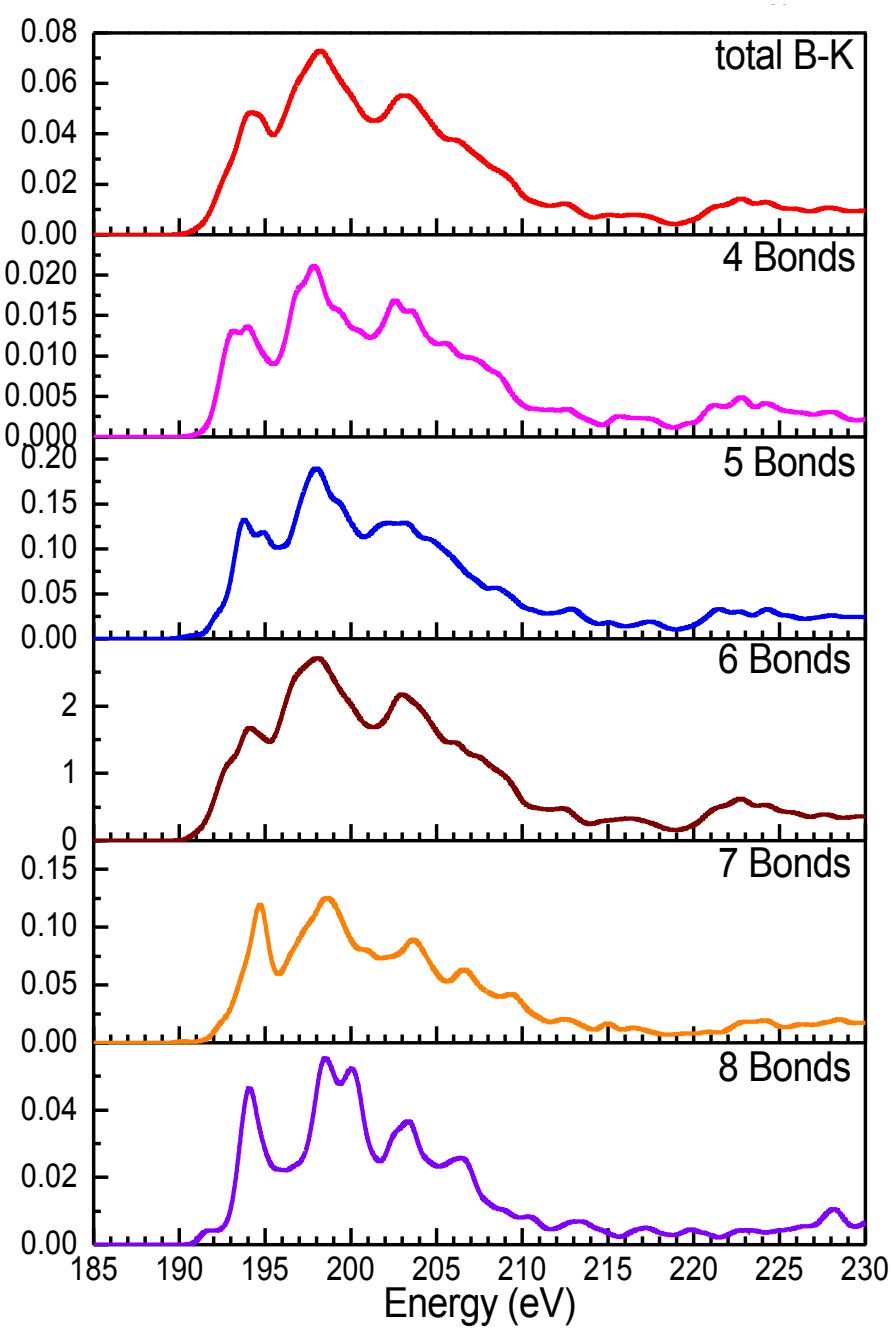

Fig.14 Bond-grouped XANES Spectra of β-B_{106}

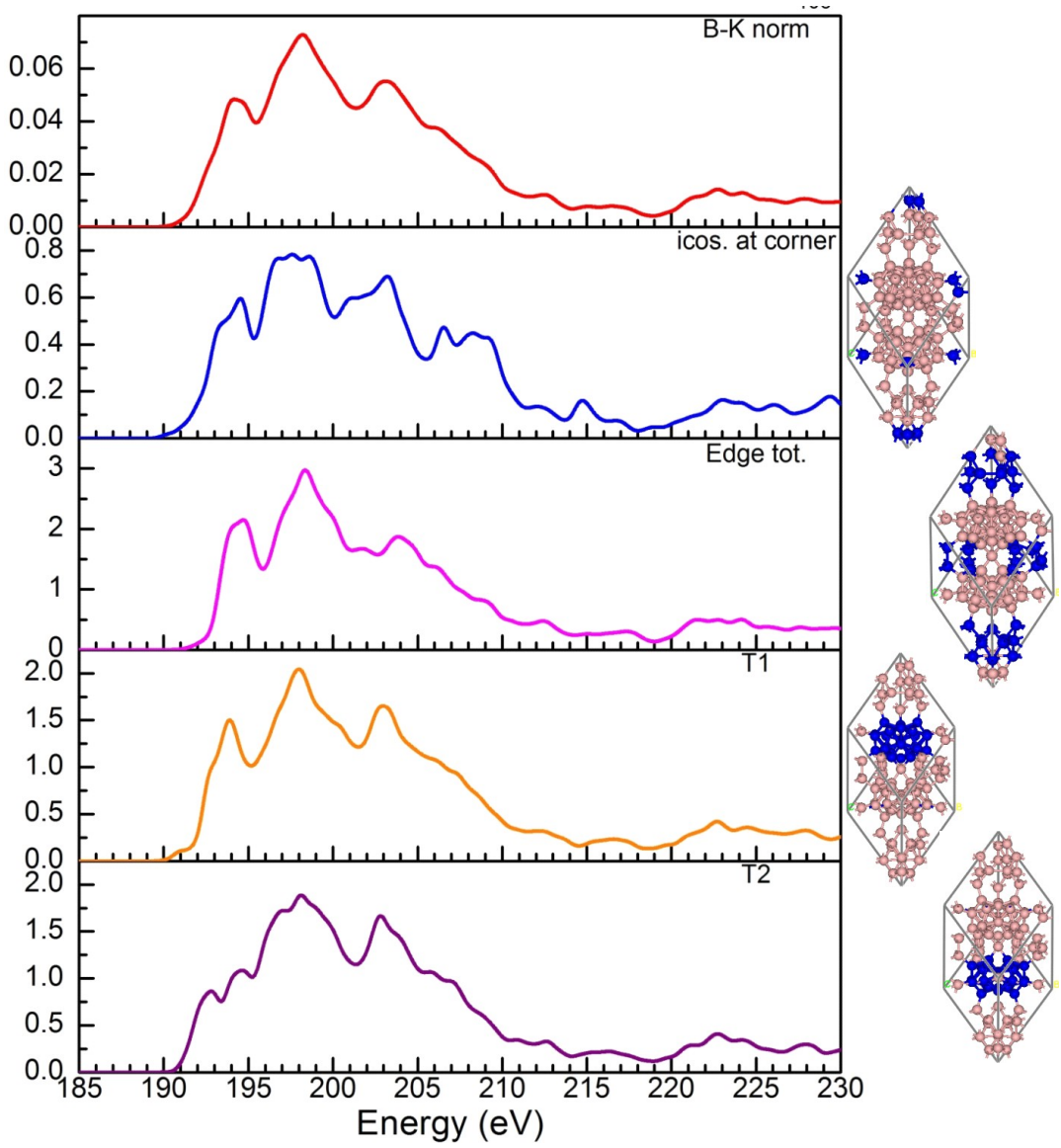

Fig.15 Unit-Grouped XANES Spectra of β-B_{106}

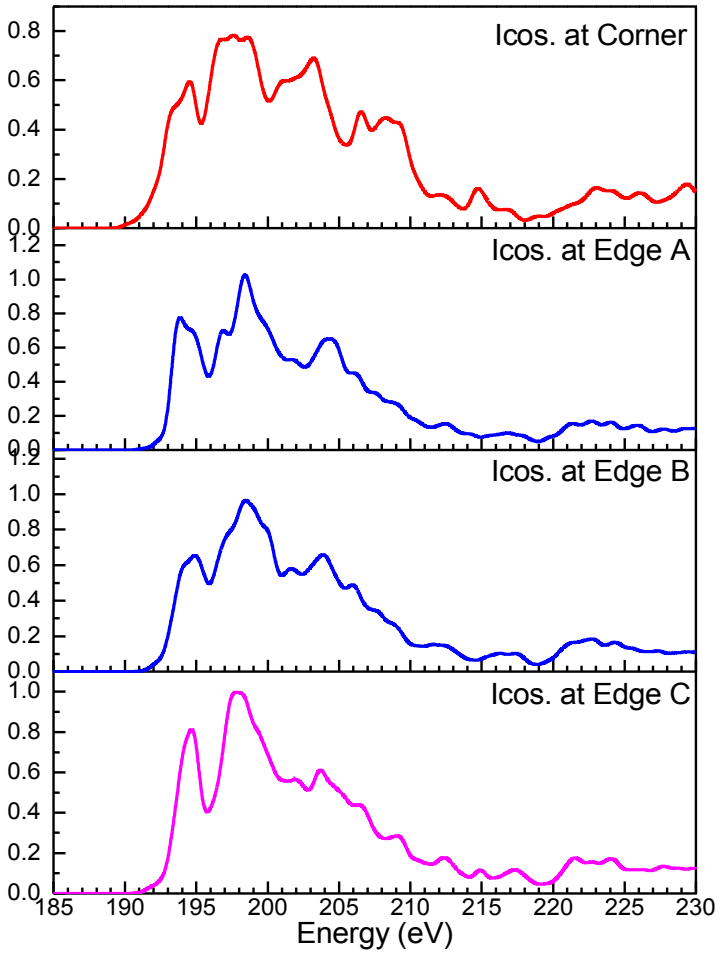

Fig.16 XANES Spectra of Single Icosahedra at Different Locations in β-B_{106}

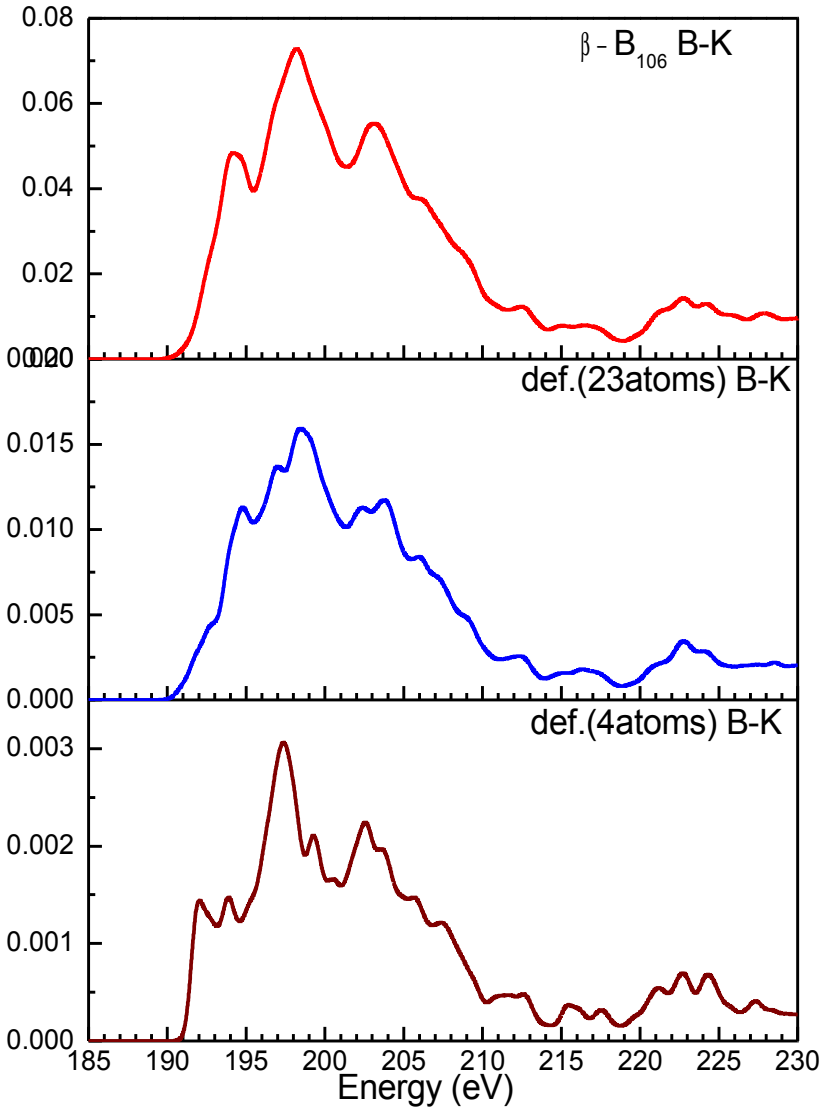

Fig.17 XANES Spectra of sites with Defective States in the Band Gap of β-B_{106}

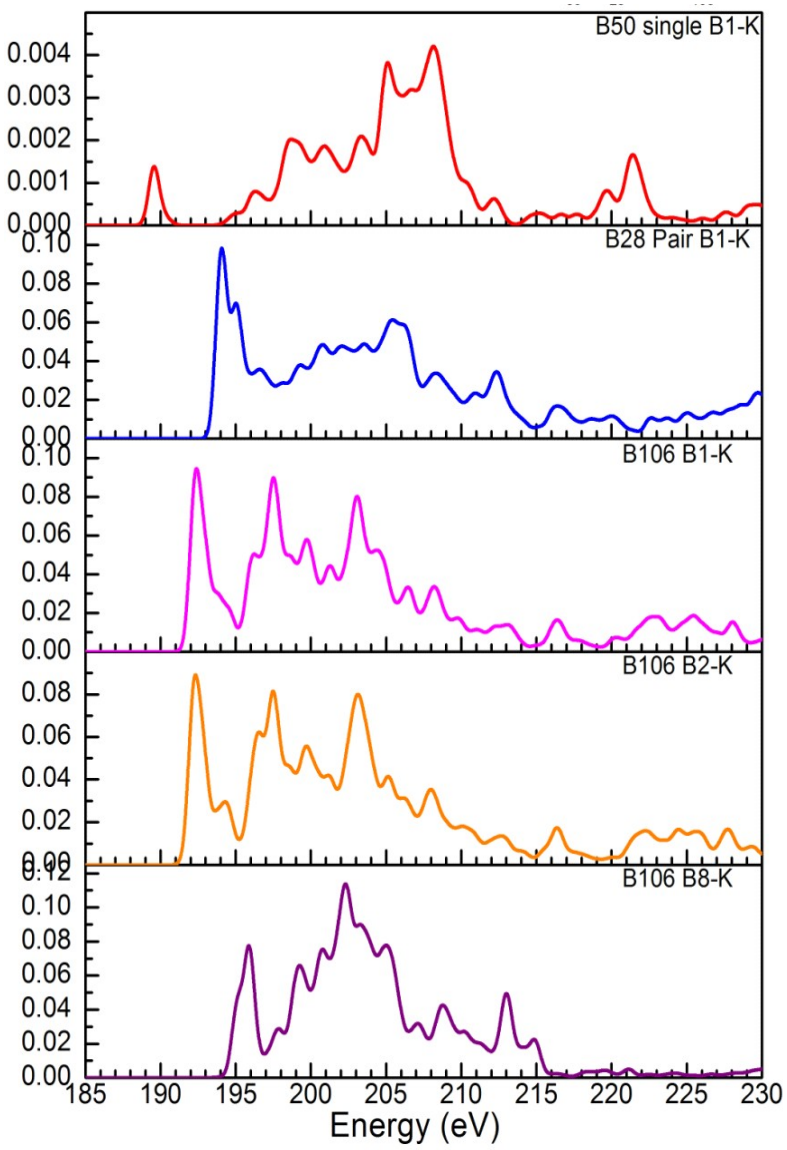

Fig.18 Grouped (single/pair boron) XANES Spectra of t-B_{50}, γ-B_{28} and β-B_{106}

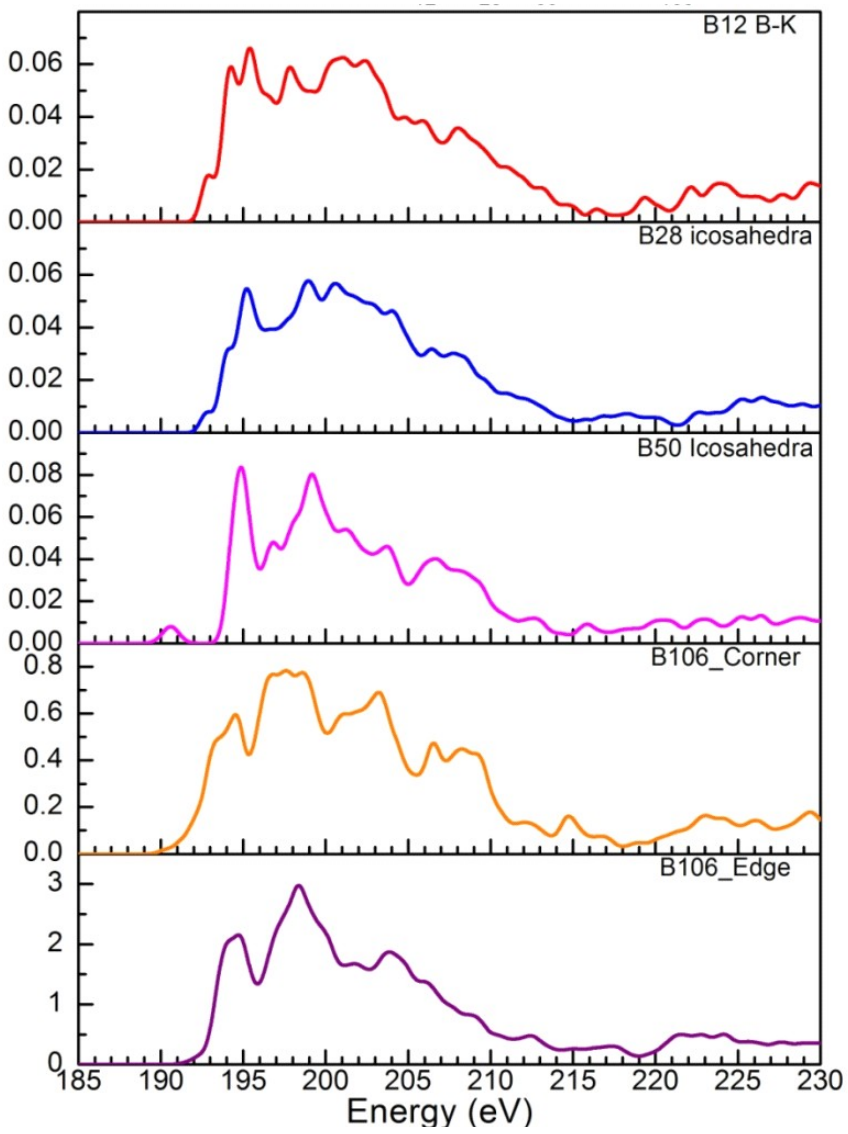

Fig.19 Grouped (icosahedra) XANES Spectra of α-B_{12},t-B_{50}, γ-B_{28} and β-B_{106}

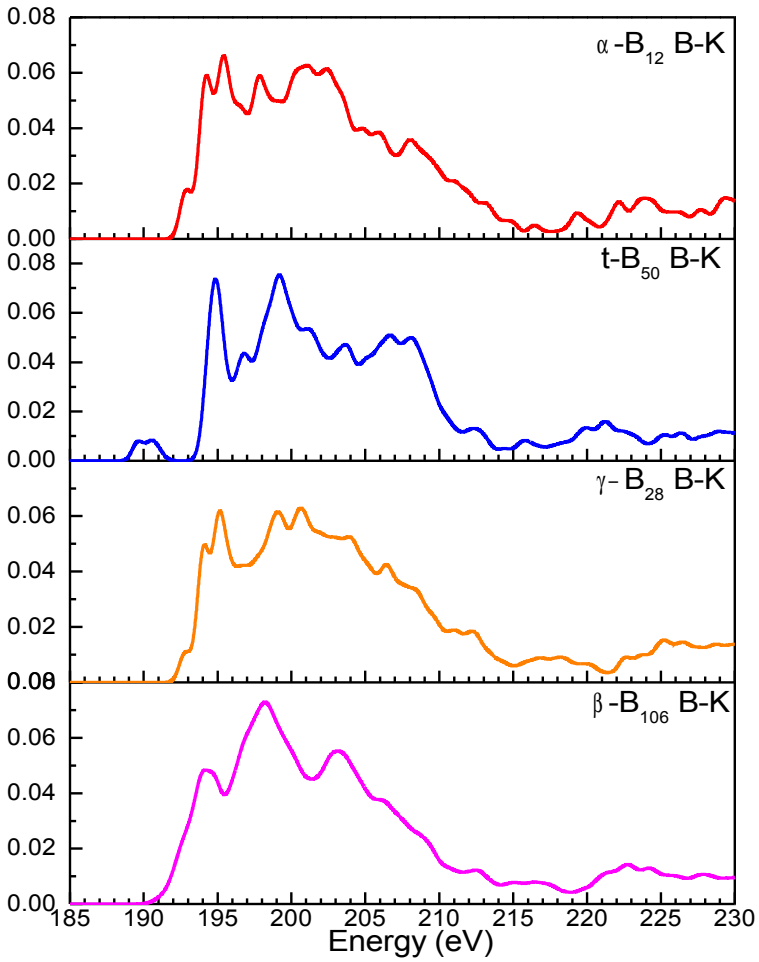

Fig.20 Total B-K Edges in α-B_{12},t-B_{50}, γ-B_{28} and β-B_{106}

Table 5 Grouped Site of β-B_{106} Based on Bond Number

Bond Number	Amount of Bond	Site-type ID
4	4	B5, B6, B85, B92
5	15	B8, B59, B60, B62, B63, B66, B67, B69, B70, B86-B91
6	65	B1-B4, B7, B11-B16, B18, B21, B23-B28, B31, B34-B46, B61, B64, B65, B68, B71-B84, B93-B106
7	13	B10, B17, B19, B20, B22, B29, B30, B32, B33, B47, B49, B50, B51
8	9	B9, B48, B52-B58

CHAPTER 4

SUMMARY AND FUTURE WORK

Elemental boron system has one element and different phases. Although boron has complex structures, the unique element does reduce the complexity of the analysis. Density of states and XANES spectra of α-B_{12}, t-B_{50}, γ-B_{28}, and β-B_{106} have been calculated by applying the super-cell OLCAO method. By comparing their properties together, we concluded that t-B_{50} is a metallic material, and that the rest are semiconductors. The density of states and partial density of states shows the distribution of different sites to the states.

XANES spectra of t-B_{50}, γ-B_{28}, and β-B_{106} are predicted based on the agreement with experimental XANES spectra of α-B_{12}. Decomposed XANES spectra of four phases are discussed and these spectra show the relation to the structural difference. XANES spectra are also discussed based on the geometrical units. From these spectra, we observed that XANES spectra are affected by local environment, such as distortion, interstitial sites, etc. Generally, the XANES spectra of all icosahedra in different crystal structures are somewhat similar. And the single "interstitial" boron atom or boron pair could be identified based on the spectra.

So far, although many efforts have been put on XANES spectra analysis, for example, grouped XANES spectra are calculated and analyzed, the understanding of XANES spectra is yet incomplete. A lot of work remains to be done. First, many papers on XANES spectra are interpreted in terms of molecular models. However, real samples are often bulk solids. It is necessary to explore how to interpret the spectra in solid state physics or quantum theory. Second, how to direct the experiment based on simulation and how to interpret experimental results more meaningfully are big challenges. These challenges direct me to future research.

REFERENCES

[1] R. Lazzari, N. Vast, J. M. Besson, S. Baroni, and A. Dal Corso, Physical Review Letters **83,** 3230 (1999).

[2] J. E. Saal, S. Shang, and Z.-K. Liu, Applied Physics Letters **91,** 231915 (2007).

[3] K.A. Schwez and A.Lipp, in *Boron Carbide, Boron Nitride and Metal Borides, in Ullman's Encyclopedia of Industrial Chemistry* (Verlag Chemie, Weinheim, 1985), p. 295.

[4] J. He, E. Wu, H. Wang, R. Liu, and Y. Tian, Physical Review Letter **94,** 015504 (2005).

[5] M. M. Balakrishnarajan, P. D. Pancharatna, and R. Hoffmann, New Journal Chemistry **31,** 473 (2007).

[6] H.Werheiit, in *Boron Compounds, in Landoldt-Bornstein, Numerical Data and Functional Relationships in Science and Technology*; *Vol. 41D*, edited by O. Madelung, M. Schulz, and H. Weiss (Springer, Berlin), p. 1.

[7] D. W. Bullett, Journal of Physics C: Solid State Physics **15,** 415 (1982).

[8] Emin, Physics Today **40,** 55 (1987).

[9] E. D. Jemmis and M. M. Balakrishnarajan, Journal of the American Chemical Society **123,** 4324 (2001).

[10] Mikhail I. Eremets, Viktor V. Struzhkin, Ho-kwang Mao, and R. J. Hemley, Science **293,** 272 (2001).

[11] S. Koun and et al., Journal of Physics: Conference Series **176,** 012001 (2009).

[12] S. Shang, Y. Wang, R. Arroyave, and Z.-K. Liu, Physical Review B (Condensed

Matter and Materials Physics) **75,** 092101 (2007).

[13] A. Masago, K. Shirai, and H. Katayama-Yoshida, Physical Review B (Condensed Matter and Materials Physics) **73,** 104102 (2006).

[14] R. Jimbou, N. Ogiwara, M. Saidoh, K. Morita, K. Mori, and B. Tsuchiya, Journal of Nuclear Materials **220-222,** 869 (1995).

[15] M. J. van Setten, M. A. Uijttewaal, G. A. de Wijs, and R. A. de Groot, Journal of the American Chemical Society **129,** 2458 (2007).

[16] K. Kajihara, H. Kamioka, M. Hirano, T. Miura, L. Skuja, and H. Hosono, Journal of Applied Physics **98,** 013529 (2005).

[17] A. N. Caruso, P. A. Dowben, S. Balkir, N. Schemm, K. Osberg, R. W. Fairchild, O. B. Flores, S. Balaz, A. D. Harken, B. W. Robertson, and J. I. Brand, Materials Science and Engineering: B **135,** 129 (2006).

[18] T. L. Aselage, D. Emin, S. S. McCready, and R. V. Duncan, Physical Review Letters **81,** 2316 (1998).

[19] V. K. Zaitsev, *Thermoelectric properties of anisotropic* $MnSi_{1.75}$ (CRC Press, Boca Raton, FL, 1995).

[20] C. G. Parazzoli, R. B. Greegor, K. Li, B. E. C. Koltenbah, and M. Tanielian, Physical Review Letters **90,** 107401 (2003).

[21] P K MacKeown and D. J. Newman, *Computational Techniques in Physics* (Adam Hilger, Bristol, 1987).

[22] *Solid State Phyiscs*; *Vol.*, edited by N. Ashcroft and D. Mermin (Thomson Learning, Inc., 2004).

[23] L. Ouyang and W. Y. Ching, Journal of Applied Physics **95,** 7918 (2004).

[24] W. Y. Ching and P. Rulis, Physical Review B (Condensed Matter and Materials Physics) **77,** 125116 (2008).

[25] H. Yao, L. Ouyang, and W.-Y. Ching, Journal of the American Ceramic Society **90,** 3194 (2007).

[26] L. Liang, P. Rulis, B. Kahr, and W. Y. Ching, Physical Review B **80,** 235132 (2009).

[27] P. Rulis, L. Wang, and W. Y. Ching, physica status solidi (RRL) - Rapid Research Letters **3,** 133 (2009).

[28] W.-Y. Ching, Journal of the American Ceramic Society **87,** 1996 (2004).

[29] D. Li, Y.-N. Xu, and W. Y. Ching, Physical Review B **45,** 5895 (1992).

[30] W. Y. Ching and P. Rulis, Physical Review B (Condensed Matter and Materials Physics) **77,** 035125 (2008).

[31] W. Y. Ching, L. Ouyang, P. Rulis, and H. Yao, Physical Review B (Condensed Matter and Materials Physics) **78,** 014106 (2008).

[32] W. Y. Ching, Journal of the American Ceramic Society **73,** 3135 (1990).

[33] S. R. Aryal, Thesis, Univeristy of Missouri- Kansas City, 2007.

[34] W.-Y. Ching and P. Rulis, Journal of Physics: Condensed Matter **21,** 104202 (2009).

[35] G. A. Slack, C. I. Hejna, M. F. Garbauskas, and J. S. Kasper, Journal of Solid State Chemistry **76,** 52 (1988).

[36] J. L. HOARD, D. B. SULLENGER, C. H. L. KENNARD, and R. E. HUGHES, JOURNAL OF SOLID STATE CHEMISTRY **1,** 268 (1970).

[37] A. R. Oganov, J. Chen, C. Gatti, Y. M. Yanzhang Ma, Colin W. Glass, Zhenxian Liu,

and O. O. K. V. L. S. Tony Yu, Nature **457,** 863 (2009).

[38] N. Vast, Phys. Rev. Lett. **78,** 693 (1997).

[39] D. R. Tallant, T. L. Aselage, A. N. Campbell, and D. Emin, Physical Review B **40,** 5649 (1989).

[40] D. D. Ebbing, *General Chemistry*, Third Edition ed. (Houghton Mifflin Company, Boston, 1990).

[41] M. Fujimori, T. Nakata, T. Nakayama, E. Nishibori, K. Kimura, M. Takata, and M. Sakata, Physical Review Letters **82,** 4452 (1999).

[42] J. L. Hoard, R. E. Hughes, and D. E. Sands, Journal of the American Chemical Society **80,** 4507 (2002).

[43] Y. Imai, M. Mukaida, M. Ueda, and A. Watanabe, Journal of Alloys and Compounds **347,** 244 (2002).

[44] B. Callmer, Acta Crystallogr. **B33,** 1951 (1977).

[45] J. L. Hoard, D. B. Sullenger, C. H. L. Kennard, and R. E. Hughes, Journal of Solid State Chemistry **1,** 268 (1970).

[46] B.Callmer, Acta Crystallographica Section B **33,** 1951 (1977).

[47] E. D. Jemmis and D. L. V. K. Prasad, Journal of Solid State Chemistry **179,** 2768 (2006).

[48] E. D. Jemmis, M. M. Balakrishnarajan, and P. D. Pancharatna, Journal of the American Chemical Society **123,** 4313 (2001).

[49] S. Hosoi, K. Tanabe, H. Kim, K. Kirihara, K. Soga, K. Kimura, K. Kato, and M. Takata, Journal of Physics: Conference Series **176,** 012026 (2009).

[50] M. A. U. Michiel J. van Setten, Gilles A. de Wijs, and Robert A. de Groot Journal of the American Chemical Society **129,** 2458 (2007).

[51] P. Villars; and L. D. Calvert, *Pearson's handbook of crystallographic data for intermetallic phases /* Vol. 2, 2 ed. (Newbury, OH : ASTM International, 1991).

[52] U. Haussermann, S. I. Simak, R. Ahuja, and B. Johansson, Physical Review Letters **90,** 065701 (2003).

[53] D. M. Bylander, L. Kleinman, and S. Lee, Physical Review B **42,** 1394 (1990).

[54] M. Terauchi, Y. Kawamata, M. Tanaka, M. Takeda, and K. Kimura, Journal of Solid State Chemistry **133,** 156 (1997).

VITA

Liaoyuan Wang was born in Hefei, Anhui Province of P.R.China. He was educated in local public schools. In 2001, he graduated from University of Science and Technology of China (USTC) and received the Bachelor degree of Management. After short work, he returned to USTC and spent three years on his graduate study. He obtained his Master degree of Science in 2006.

In September 2007, Mr. Wang came to the United States as a PhD student in the department of Physics at the University of Missouri-Kansas City. He also worked as Teaching assistant. He was qualified as PhD candidates in 2008.

Mr. Wang is a member of the American Physical Society. He has published one paper in physica status solidi (RRL) -Rapid Research Letters. He was outstanding student for oral presentation in the 34th ICACC conference in 2010.